Electrical and Computer Engineering Publications | Dept. of Electrical and Computer Engineering

2004

Phase-coherent quantum mechanical spin transport in a weakly disordered quasi-one-dimensional channel

M. Cahay
University of Cincinnati - Main Campus

S. Bandyopadhyay
Virginia Commonwealth University, sbandy@vcu.edu

Phase-coherent quantum mechanical spin transport in a weakly disordered quasi-one-dimensional channel

M. Cahay*

Department of Electrical and Computer Engineering and Computer Science, University of Cincinnati, Cincinnati, Ohio 45221, USA

S. Bandyopadhyay

Department of Electrical Engineering, Virginia Commonwealth University, Richmond, Virginia 23284, USA

A transfer matrix technique is used to model phase-coherent spin transport in the weakly disordered quasi-one-dimensional channel of a gate-controlled electron spin interferometer [S. Datta and B. Das, Appl. Phys. Lett. **56**, 665 (1990)]. The model includes the effects of an axial magnetic field in the channel of the interferometer (caused by the ferromagnetic contacts), a Rashba spin-orbit interaction, and elastic (nonmagnetic) impurity scattering. We show that in the presence of an axial magnetic field, nonmagnetic impurities can cause spin relaxation in a manner similar to the Elliott-Yafet mechanism. The amplitudes and phases of the conductance oscillations of the interferometer and the degree of spin-conductance polarization are found to be quite sensitive to the height of the interface barrier at the contact, as well as the strength, locations, and nature (attractive or repulsive) of just a few elastic nonmagnetic impurities in the channel. This can seriously hinder practical applications of spin interferometers.

I. INTRODUCTION

In a seminal paper published in 1990, Datta and Das[1] proposed a gate-controlled electron spin interferometer which is an analog of the standard electro-optic light modulator. Their device consists of a one-dimensional semiconductor channel with ferromagnetic source and drain contacts (Fig. 1). Electrons are injected into the channel from the ferromagnetic source with a definite spin, which is then controllably precessed in the channel with a gate-controlled Rashba interaction[2] and finally sensed at the drain. At the drain end, the electron's transmission probability depends on the relative alignment of its spin with the drain's (fixed) magnetization. By controlling the angle of spin precession in the channel with a gate voltage, one can modulate the relative spin alignment at the drain end and, hence, control the source-to-drain current (or conductance). In this device, the ferromagnetic source and drain contacts act as "spin polarizer" and "spin analyzer," respectively.

There have been some studies of ballistic spin transport in such a device,[3–6] but they ignored two features that are always present in a real device structure. First, there is an axial magnetic field along the channel caused by the ferromagnetic contacts. This field dramatically alters the dispersion relations of the subbands in the channel, causes spin mixing, and has a serious effect on spin transport. Second, even though there have been reports of several microns long nearly defect-free one-dimensional quantum wires formed in high-quality modulation doped GaAs/AlGaAs heterostructures,[7] it is likely that in circuits involving a large number of spin interferometers, some of them will have a few impurities in the channel. We show that these impurities, even if they are nonmagnetic, can cause spin relaxation in the presence of the axial magnetic field. Thus, they can affect the conductance modulation of the interferometer and the degree of spin polarization of the current.

This paper is organized as follows. In the next section, we describe the Hamiltonian to model the gate-controlled electron spin interferometer depicted in Fig. 1. The Hamiltonian includes potential barriers at the contact/channel interface that are inevitably present, the axial magnetic field, and localized impurities in the channel. It does not include pertur-
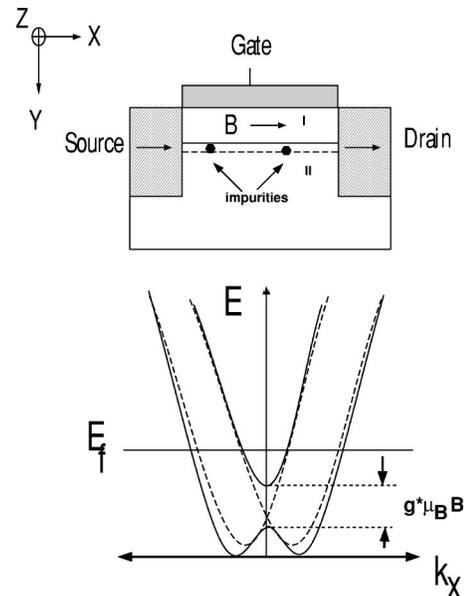
FIG. 1. A schematic of the electron spin interferometer from Ref. 1. The horizontal dashed line represents the quasi-one-dimensional electron gas formed at the semiconductor interface between materials I and II. The magnetization of the ferromagnetic contacts is assumed to be along the $+x$ direction which results in a magnetic field along the x direction. Also shown is a qualitative representation of the energy dispersion of the two perturbed (solid line) and unperturbed (broken line) bands under the gate—the perturbation is due to the axial magnetic field along the channel.

bations due to phonons and other time-dependent scattering potentials (we assume that the channel is shorter than the phase breaking length so that transport is phase coherent). Using a truncated form of this Hamiltonian, we derive the dispersion relations of the subbands in the channel. Because of the presence of the axial magnetic field, the subbands are not eigenstates of the spin operator. Therefore, no subband has a definite spin quantization axis. Furthermore, eigenspinors in two subbands (at the same energy) are *not* orthogonal. As a result, elastic (nonmagnetic and spin-independent) impurity scattering can couple two subband states with nonorthogonal eigenspinors, causing elastic intersubband transitions that *relax spin*. One should compare this mechanism of spin relaxation with the Elliott-Yafet spin relaxation mechanism[8] in a bulk semiconductor. The Elliott-Yafet relaxation comes about because in a real crystal, the Bloch states are not eigenstates of spin so that an "upspin" state has some "downspin" component and vice versa. As a result, nonmagnetic impurity scattering can connect (mostly) up-spin and (mostly) down-spin electrons, leading to a spin relaxation. Our mechanism is very similar.

Section III contains numerical examples of the conductance modulation of a spin interferometer as a function of applied gate potential, spin polarization of the current through the channel, and effects of the interface barriers and elastic (nonmagnetic) impurity scattering. Finally, Sec. IV contains our conclusions.

II. THEORETICAL MODEL

We first consider the quasi-one-dimensional semiconductor channel of a spin interferometer in the absence of any impurities. The channel is along the x axis (Fig. 1) and the gate electric field is applied along the y direction to induce a Rashba spin-orbit coupling in the channel. This system is described by the single-particle effective-mass Hamiltonian[9,10]

$$
\mathcal{H} = (\vec{p} + e\vec{A}) \frac{1}{2m^*(x)} (\vec{p} + e\vec{A}) + V_I(x) + V_1(y) + V_2(z)
$$
$$
- (g^*/2)\mu_B \vec{B} \cdot \vec{\sigma} + \frac{1}{2}\left[\frac{\alpha_R(x)}{\hbar}\hat{y}\cdot\{\vec{\sigma}\times(\vec{p}+e\vec{A})\} + \text{H.c.}\right],
$$
$$(1)$$

where H.c. denotes Hermitian conjugate. This form of the Hamiltonian guarantees Hermiticity.[9] Here, $\hat{y}$ is the unit vector along the y direction in Fig. 1 and $\vec{A}$ is the vector potential due to the axial magnetic field $\vec{B}$ along the channel (x direction) caused by the ferromagnetic contacts. For quasi-one-dimensional channels of submicron length, it is reasonable to assume that $\vec{B}$ is homogeneous and directed along the channel's length (in other words fringing fields are not an issue). In Eq. (1), μ_B is the Bohr magneton ($e\hbar/2m_0$) and g^* is the effective Landé g factor of the electron in the channel. The quantity α_R is the Rashba spin-orbit coupling strength which depends on the gate electric field and can be varied with the gate potential. The confining potentials along the y

and z directions are denoted by $V_1(y)$ and $V_2(z)$, with the latter being parabolic in space and the former will be approximately triangular. We assume that $V_1(y)$ is strong enough that only one subband along the y direction is occupied by electrons.

Since the potential $V_2(z)$ is parabolic, it results in a spatially varying electric field along the z direction. This electric field might have contributed additional Rashba spin-orbit coupling terms in Eq. (1). However, since the potential $V_2(z)$ is *symmetric* about the origin of the parabola, for every electric field at a coordinate point z, there is an equal and opposite electric field at coordinate $-z$. The Rashba coupling constant α_R is the product of a material-specific constant a_{46} (Ref. 11) and the *expectation value* of the electric field in the z direction (Ref. 12). This expectation value is zero because the spatial average of the electric field along the z direction vanishes. Hence, there is no overall Rashba effect associated with $V_2(z)$. Therefore, we have considered only the contribution of the gate electric field (applied in the y direction) to the Rashba effect in the channel.

In Eq. (1), $V_I(x)$ represents an interfacial potential barrier between the metallic ferromagnetic contacts and the semiconducting channel. This potential could come about from several sources. For example, Schäpers *et al.*[13] used a δ-function potential at the interface to represent a tunnel barrier that can facilitate coherent spin injection across a metallic ferromagnet and a semiconducting paramagnet interface.[14] Alternately, this potential could also represent a very narrow contact potential associated with Ohmic contacts. An Ohmic contact forms when the semiconductor material in the neighborhood of the metal contact has a large carrier concentration so that the Schottky barrier at the metal/semiconductor interface becomes very narrow and electrons from the contact tunnel easily through this into the semiconducting channel, resulting in a very small contact resistance or an Ohmic contact. Following Schäpers *et al.*,[13] we model these interface barriers as δ barriers given by

$$
V_I(x) = V_L \delta(x) + V_R \delta(x-L), \tag{2}
$$

where V_L and V_R are assumed equal.

In Eq. (1), we have neglected a few effects for the sake of simplicity. We have neglected the normal Elliott-Yafet interaction[8] because it is weak in quasi-one-dimensional structures (where elastic scattering is strongly suppressed[15]). We have also neglected the Dresselhaus interaction[16] since it does not relax spin when the initial spin polarization is along the axis of the wire[17–20] (this is the case with the gate-controlled spin interferometer). The Dresselhaus interaction can, however, be easily included in the Hamiltonian and is left for future work. Finally, we model localized nonmagnetic impurities (i.e., which do not flip the spin) using a standard model of δ scatterers. The scattering potential is given by

$$
V_{imp} = \sum_{i=1}^{N} \Gamma_i \delta(x-x_i) \tag{3}
$$

to represent N impurities in the channel at location x_i and with strength Γ_i (assumed to be spin independent). In our

numerical examples, we consider the case of both attractive (Γ_i negative) and repulsive (Γ_i positive) impurities. While Eq. (1) represents a ballistic channel with no scattering, addition of the scattering potential in Eq. (3) to Eq. (1) will result in a Hamiltonian describing a weakly disordered channel in which impurity scattering takes place. The eigenstates of this (spin-dependent) Hamiltonian can then be found using a transfer matrix technique to extract the electron wave function in the presence of impurity scatterers. From this wave function, we can calculate the (spin-dependent) transmission probability through the channel and ultimately the (spin-dependent) channel conductance.

Let us now concentrate on the channel region between $x=0$ and $x=L$ (see Fig. 1). The choice of the Landau gauge $\vec{A}=(0,-Bz,0)$ allows us to decouple the y component of the Hamiltonian in Eq. (1) from the x-z component in the channel. Furthermore, if we ignore V_{imp} for the moment, the solution of the Schrödinger equation in the channel can be written as a linear superposition of left and right traveling plane waves (V_{imp} will couple various wave vector states which is handled by the transfer matrix technique described later). The two-dimensional Hamiltonian in the plane of such a ballistic channel (x-z plane) is then given by

$$H_{xz} = \frac{p_z^2}{2m^*} + \Delta E_c + \frac{1}{2}m^*(\omega_0^2+\omega_c^2)z^2 + \frac{\hbar^2 k_x^2}{2m^*} + \frac{\hbar^2 k_R k_x}{m^*}\sigma_z$$

$$-(g^*/2)\mu_B B\sigma_x - \frac{\hbar k_R p_z}{m^*}\sigma_x, \tag{4}$$

where ω_0 is the curvature of the confining potential in the z direction, $\omega_c = eB/m^*$, $k_R = m^*\alpha_R/\hbar^2$, and ΔE_c is the potential barrier between the ferromagnet and semiconductor. We assume that ΔE_c includes the effects of the quantum confinement in the y direction.

A few words are in order regarding Eq. (4). First, the effective mass is spatially invariant within the channel which is why the effective mass is treated as a constant in Eq. (4). Of course, there is a discontinuity in the effective mass at the interface with the ferromagnetic contacts at $x=0$ and $x=L$. This has been taken into account in the boundary conditions [see Eqs. (17) and (18)]. Second, α_R is also spatially invariant in the homogeneous channel because the material constant a_{46} is invariant. Therefore, $\nabla \alpha_R$ terms [arising from the Hermitian conjugate terms in Eq. (1)] vanish in the channel and do not appear in Eq. (4)). However, the discontinuities in α_R at the interfaces between the semiconductor channel and the ferromagnetic contacts will lead to two δ-function spin-orbit coupling terms at $x=0$ and $x=L$. These are like the interface potential V_I and have been accounted for via the boundary conditions [see Eqs. (17) and (18) later].

A. Energy dispersion relations

We now derive the energy dispersion relations in the channel of a ballistic interferometer using Eq. (4). The first five terms of the Hamiltonian in Eq. (4) yield shifted parabolic subbands with dispersion relations

$$E_{n,\uparrow} = (n+1/2)\hbar\omega + \Delta E_c + \frac{\hbar^2 k_x^2}{2m^*} + \frac{\hbar^2 k_R k_x}{m^*},$$

$$E_{n,\downarrow} = (n+1/2)\hbar\omega + \Delta E_c + \frac{\hbar^2 k_x^2}{2m^*} - \frac{\hbar^2 k_R k_x}{m^*}, \tag{5}$$

where $\omega = \sqrt{\omega_0^2 + \omega_c^2}$. In Eq. (5), the $\uparrow$ and $\downarrow$ arrows indicate $+z$- and $-z$-polarized spins (eigenstates of the σ_z operator) which are split by the Rashba effect [fifth term of the Hamiltonian in Eq. (4)]. These are subbands with definite spin quantization axes along the $+z$ and $-z$ directions since they are eigenstates of the σ_z operator. Their dispersion relations are shown as dashed lines in Fig. 1.

The sixth and seventh terms in Eq. (4) induce a perturbation and mixing between the unperturbed subbands ($+z$- and $-z$-polarized spins). The sixth term originates from the magnetic field due to the ferromagnetic contacts and the seventh originates from the Rashba effect itself. The ratio of these two terms can be shown to be of the order of 10^4–10^6 for typical values of the relevant parameters. Therefore, we can neglect the seventh term in comparison with the sixth term (for a very strong Rashba effect, much stronger than what has been experimentally observed in semiconductor structures, the seventh term can also matter and introduce additional spin mixing effects[21]).

To obtain an analytical expression for the dispersion relation corresponding to the first six terms in the Hamiltonian in Eq. (4), we derive the two-band dispersion relation in a truncated Hilbert space considering mixing between the two lowest unperturbed subband states (namely, the $+z$ and $-z$ spin states). Straightforward diagonalization of the Hamiltonian in Eq. (4) (minus the seventh term) in the basis of these two unperturbed states gives the following dispersion relations:

$$E_1(k_x) = \frac{1}{2}\hbar\omega + \Delta E_c + \frac{\hbar^2 k_x^2}{2m^*} - \sqrt{\left(\frac{\hbar^2 k_R k_x}{m^*}\right)^2 + \left(\frac{g^*\mu_B B}{2}\right)^2}, \tag{6}$$

$$E_2(k_x) = \frac{1}{2}\hbar\omega + \Delta E_c + \frac{\hbar^2 k_x^2}{2m^*} + \sqrt{\left(\frac{\hbar^2 k_R k_x}{m^*}\right)^2 + \left(\frac{g^*\mu_B B}{2}\right)^2}, \tag{7}$$

where the indices 1 and 2 refer to the lower and upper subbands. Their dispersion relations are plotted schematically as solid lines in Fig. 1.

One can see from Fig. 1 that the magnetic field caused by the ferromagnetic contacts couples the two unperturbed subbands (the original $+z$- and $-z$-polarized subbands) and changes their dispersion relation, lifting the degeneracy at $k_x=0$. While the unperturbed bands are shifted parabolas with single minima at $k_x = \pm k_R$,[1] the perturbed bands (in the presence of a magnetic field) are not parabolic and are symmetric about the energy axis. One of them has a single minimum at $k_x=0$, and the other has double minima at $k_x = \pm k_R\sqrt{1+(g^*\mu_B B/\delta_R)^2}$, where $\delta_R = \hbar^2 k_R^2/2m^*$. The magnetic field not only has this profound influence on the dispersion relations, but it also causes *spin mixing*, meaning that the perturbed subbands no longer have definite spin quantization axes (they are no longer $+z$- and $-z$-polarized sub-

bands) because they are no longer eigenstates of the spin operator. Spin quantization becomes wave vector dependent. Furthermore, energy-degenerate states in the two perturbed subbands no longer have orthogonal spins. Therefore, elastic scattering between them is possible without a complete spin flip.

The energy dispersion relations also show that the difference Δk_x between the wave vectors in the two subbands at any given energy is *not* independent of that energy. Since Δk_x is proportional to the angle by which the spin precesses in the channel,[1] the angle of spin precession in the channel of a spin interferometer is *no longer* independent of electron energy. Thus different electrons that are injected from the contact with different energies (at finite temperature and bias) will undergo different degrees of spin precession, and the conductance modulation will not survive ensemble averaging over a broad spectrum of electron energy at elevated temperatures and bias. In Ref. 1, which did not consider the effect of the axial magnetic field, a point was made that the angle of spin precession is independent of electron energy so that every electron undergoes the same degree of spin precession in the channel irrespective of its energy. As a result, the conductance modulation of the spin interferometer is not diluted by ensemble averaging over electron energy at elevated temperature and bias. Indeed this is true in the absence of an axial magnetic field, but when a magnetic field is considered, this advantage is lost.

From Eqs. (6) and (7), we find that an electron incident with total energy E has wave vectors in the two channel subbands given by

$$k_{x\pm} = \frac{1}{\hbar}\sqrt{2m^*\left(\frac{B \pm \sqrt{B^2 - 4C}}{2}\right)}, \qquad (8)$$

where

$$B = 2\left(E - \frac{\hbar\omega}{2} - \Delta E_c\right) + 4\delta_R, \quad C = \left(E - \frac{\hbar\omega}{2} - \Delta E_c\right)^2 - \beta^2, \qquad (9)$$

with $\beta = g^*\mu_B B/2$.

In Eq. (8), the upper and lower signs correspond to the lower and upper subbands in Fig. 1 and are referred to hereafter as $k_{x,1}$ and $k_{x,2}$, respectively. The corresponding eigenspinors in the two subbands (at energy E) are, respectively,

$$\begin{bmatrix} C_1(k_{x,1}) \\ C_1'(k_{x,1}) \end{bmatrix} = \begin{bmatrix} -\alpha(k_{x,1})/\gamma(k_{x,1}) \\ \beta/\gamma(k_{x,1}) \end{bmatrix} = \begin{bmatrix} -\sin(\theta_{k_{x,1}}) \\ \cos(\theta_{k_{x,1}}) \end{bmatrix},$$

$$\begin{bmatrix} C_2(k_{x,2}) \\ C_2'(k_{x,2}) \end{bmatrix} = \begin{bmatrix} \beta/\gamma(k_{x,2}) \\ \alpha(k_{x,2})/\gamma(k_{x,2}) \end{bmatrix} = \begin{bmatrix} \cos(\theta_{k_{x,2}}) \\ \sin(\theta_{k_{x,2}}) \end{bmatrix}, \qquad (10)$$

where the quantities α and γ are functions of k_x and are given by

$$\alpha(k_x) = \frac{\hbar^2 k_R k_x}{m^*} + \sqrt{\left(\frac{\hbar^2 k_R k_x}{m^*}\right)^2 + \beta^2}, \quad \gamma(k_x)$$

$$= \sqrt{\alpha^2(k_x) + \beta^2}, \quad \theta_{k_x} = \arctan[\alpha(k_x)/\beta]. \quad (11)$$

Note that the eigenspinors given by Eq. (10) are not a $+z$-polarized state $[1\ 0]^\dagger$ or $-z$-polarized state $[0\ 1]^\dagger$ if the magnetic field $B \neq 0$ (i.e., $\beta \neq 0$). Thus, the magnetic field mixes spins and the $+z$- or $-z$-polarized states are no longer eigenstates in the channel [in other words, the subbands in Eqs. (6) and (7) are not eigenstates of the σ_z operator unlike the subbands in Eq. (5) and hence they are not $+z$- and $-z$-polarized subbands]. Equations (10) also show that the spin quantization (eigenspinor) in any subband is not fixed and strongly depends on the wave vector k_x. Thus, an electron entering the semiconductor channel from the left ferromagnetic contact with $+x$-polarized spin will not couple *equally* to $+z$ and $-z$ states. The relative coupling will depend on the electron's wave vector (or energy).

Most importantly, the two eigenspinors given by Eq. (10) are *not* orthogonal. Thus, a spin-independent elastic scatterer (nonmagnetic impurity) can couple these two subbands in the channel and cause elastic intersubband transitions. Another way of stating this is that the actual subband states are not eigenstates of the spin operator; hence, scattering between them is possible via a spin-independent scatterer. This is exactly similar to the Elliott-Yafet mechanism in a bulk crystal. Such a scattering is of course harmful for the gate-controlled spin interferometer since it introduces a random component to the spin precession in the channel. In our transfer matrix model (described later) this mechanism of scattering is automatically included since we use the actual eigenspinors in the channel given by Eq. (10) to construct the wave function (see Sec. II B later).

We model the ferromagnetic contacts by the Stoner-Wohlfarth model. The $+x$-polarized spin (majority carrier) and $-x$-polarized spin (minority carrier) band bottoms are offset by an exchange splitting energy Δ (Fig. 2). Since the interface barriers for the two types of spin are different by the amount Δ, the transmission amplitudes for the two types will be different, leading to some degree of spin-polarized injection and detection.[22]

B. Transmission through the interferometer

In this subsection, we calculate the total transmission coefficient through the spin interferometer for an electron of energy E entering the semiconductor channel from the left ferromagnetic contact (region I, $x \leq 0$) and exiting at the right ferromagnetic contact (region III, $x \geq L$). A rigorous treatment of this problem would require an accurate modeling of the three-to one-dimensional transition between the bulk ferromagnetic contacts (regions I and III) and the quantum wire semiconductor channel (region II).[23,24] However, a one-dimensional transport model to calculate the transmission coefficient through the structure is known to be a very good approximation when the Fermi wave number in the ferromagnetic contacts is much greater than the inverse of

the transverse dimensions of the quantum wire.[25,26] This is always the case with metallic contacts.

In the semiconductor channel (region II, $0 < x < L$), the x component of the wave function at a position x along the channel is given by

$$\psi_{II}(x) = A_I(E) \begin{bmatrix} C_1(k_{x,1}) \\ C_1'(k_{x,1}) \end{bmatrix} e^{ik_{x,1}x} + A_{II}(E)$$

$$\times \begin{bmatrix} C_1(-k_{x,1}) \\ C_1'(-k_{x,1}) \end{bmatrix} e^{-ik_{x,1}x} + A_{III}(E) \begin{bmatrix} C_2(k_{x,2}) \\ C_2'(k_{x,2}) \end{bmatrix} e^{ik_{x,2}x}$$

$$+ A_{IV}(E) \begin{bmatrix} C_2(-k_{x,2}) \\ C_2'(-k_{x,2}) \end{bmatrix} e^{-ik_{x,2}x}. \tag{12}$$

For a $+x$-polarized spin (majority carrier) in the left ferromagnetic contact (region I, $x < 0$), the electron is spin polarized in the $[11]^\dagger$ subband and the x component of the wave function is given by

$$\psi_I(x) = \frac{1}{\sqrt{2}} \begin{bmatrix} 1 \\ 1 \end{bmatrix} e^{ik_x^u x} + \frac{R_1(E)}{\sqrt{2}} \begin{bmatrix} 1 \\ 1 \end{bmatrix} e^{-ik_x^u x}$$

$$+ \frac{R_2(E)}{\sqrt{2}} \begin{bmatrix} 1 \\ -1 \end{bmatrix} e^{-ik_x^d x}, \tag{13}$$
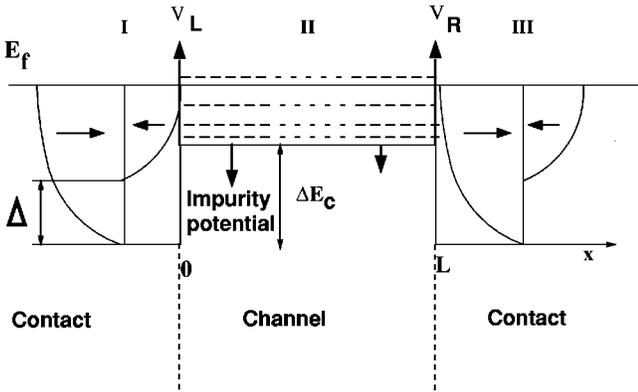

FIG. 2. Energy band diagram across the electron spin interferometer. We use a Stoner-Wohlfarth model for the ferromagnetic contacts. Δ is the exchange splitting energy in the contacts. ΔE_c is the height of the potential barrier between the energy band bottoms of the semiconductor and the ferromagnetic electrodes. ΔE_c takes into account the effects of the quantum confinement in the y and z directions. Also shown as dashed lines are the resonant energy states above ΔE_c. Peaks in the conductance of the electron spin interferometer are expected when the Fermi level in the contacts lines up with the resonant states. The barriers at the ferromagnet/semiconductor interface are modeled as simple one-dimensional δ potentials. The impurity potentials are also modeled as δ potentials at random locations (here we show attractive impurities because the δ potentials are negative).

where $R_1(E)$ is the reflection amplitude into the $+x$-polarized band and $R_2(E)$ is the reflection amplitude in the $-x$-polarized band for an electron incident with energy E.

In the right ferromagnetic contact (region III, $x > L$), the x component of the wave function is given by

$$\psi_{III}(x) = \frac{T_1(E)}{\sqrt{2}} \begin{bmatrix} 1 \\ 1 \end{bmatrix} e^{ik_x^u(x-L)} + \frac{T_2(E)}{\sqrt{2}} \begin{bmatrix} 1 \\ -1 \end{bmatrix} e^{ik_x^d(x-L)}, \tag{14}$$

where $T_1(E)$ and $T_2(E)$ are the transmission amplitudes into the $+x$- and $-x$-polarized bands in the right contact. In Eqs. (13) and (14), the wave vectors

$$k_x^u = \frac{1}{\hbar}\sqrt{2m_0 E}, \quad k_x^d = \frac{1}{\hbar}\sqrt{2m_0(E-\Delta)} \tag{15}$$

are the x components of the wave vectors corresponding to energy E in the majority ($+x$-polarized) and minority ($-x$-polarized) spin bands, respectively.

If there are impurities in the channel, we must write a solution to the Schrödinger equation in each "ballistic" segment of the channel between neighboring impurities in the form given by Eq. (12) with different values for the coefficients $A_i(E)(i=1,4)$. In addition to the continuity of the wave function across each impurity in the channel, the following condition must be satisfied, which is obtained through an integration of the Schrödinger equation across the impurity:

$$\frac{d\psi}{dx}(x_i+\epsilon) = \frac{d\psi}{dx}(x_i-\epsilon) + \frac{2m^*\Gamma_i}{\hbar^2}\psi(x_i). \tag{16}$$

Furthermore, because of the interfacial barrier at the two ferromagnet/semiconductor contacts, the integration of the Schrödinger equation across the left and right interface regions leads to the following two boundary conditions:

At $x=0$,

$$\mu\frac{d\psi}{dx}(-\epsilon) + \frac{2m^*V_0}{\hbar^2}\psi(0) = \frac{d\psi}{dx}(+\epsilon) + ik_R(+\epsilon)\sigma_z\psi(+\epsilon), \tag{17}$$

and, at $x=L$,

$$\mu\frac{d\psi}{dx}(L+\epsilon) - \frac{2m^*V_0}{\hbar^2}\psi(L) = \frac{d\psi}{dx}(L-\epsilon)$$

$$+ ik_R(L-\epsilon)\sigma_z\psi(L), \tag{18}$$

where V_0 is determined by V_I and ΔE_c, $\mu = m_s^*/m_f^*$, and m_s^* and m_f^* are the effective masses in the semiconductor and ferromagnetic materials, respectively. Here, we have made use of the fact that α_R (and therefore k_R) is zero in the ferromagnetic contacts so that terms containing $k_R(-\epsilon)$ and $k_R(L+\epsilon)$ do not appear in Eqs. (17) and (18). Equations (17)

and (18) ensure continuity of the current density at the ferromagnetic contact/semiconductor interface.

For the case of N impurities in the channel, the equations above lead to a system of $4(N+2)$ equations with $4(N+2)$ unknowns [$R_1(E)$, $R_2(E)$, $T_1(E)$, $T_2(E)$ and $N+1$ sets of $A_i(E)(i=\text{I,II,III,IV})$ for the $N+1$ regions in the channel demarcated by the N impurities]. This system of equations must then be solved to find the transmission probabilities $T_1(E)$ and $T_2(E)$. The problem is repeated for two cases: (i) when the initial spin is $+x$ polarized (i.e., the incoming electron is a majority carrier in the left contact) and (ii) when the incoming electron is $-x$ polarized (i.e., the incident electron is a minority carrier in the left contact). Finally, the linear response conductance of the spin interferometer (for injection from either the $+x$- or $-x$-polarized bands in the left contact) is found from the Landauer formula

$$G_{+x\text{-polarized}}=\frac{e^2}{4hkT}\int_0^\infty dE\,|T_{tot}(E)|^2\text{sech}^2\left(\frac{E-E_F}{2kT}\right),$$

(19)

where

$$|T_{tot}(E)|^2=|T_1(E)|^2+(k_x^d/k_x^u)|T_2(E)|^2.$$

(20)

Similarly, the conductance of the minority spin carriers ($G_{-x\text{-polarized}}$) is calculated after repeating the scattering problem for electrons incident from the minority spin band in the contacts. Since the $+x$- and $-x$-polarized spin states are orthogonal in the contacts, the total conductance of the spin interferometer is given by

$$G=G_{+x\text{-polarized}}+G_{-x\text{-polarized}}.$$

(21)

C. Role of the interface potentials

The interface potentials V_I determine V_0 and the solutions of the Schrödinger equation and, therefore, the transmission probabilities and conductance. To elucidate the role of V_I, we introduce the following parameter:

$$Z=\frac{2m_f^*V_0}{\hbar^2}.$$

(22)

Typical values of Z vary in the range of 0–2.[13] Using $m_f^*=m_0$ and $k_F=1.05\times10^8$ cm^{-1}, we get a barrier strength $V_0=16$ eV Å for $Z=2$. In the next section, we will show how the conductance modulation of the spin interferometer depends on Z.

III. NUMERICAL EXAMPLES

We consider a spin interferometer consisting of a quasi-one-dimensional InAs channel between two ferromagnetic contacts. The electrostatic potential in the z direction is assumed to be harmonic [with $\hbar\omega=10$ meV in Eq. (4)]. We assume a g^* factor of 3 and an electron effective mass $m^*=0.036m_0$ which is typical of InAs-based channels.[12] We also assume that the magnetic field along the channel is 1 T

based on an estimate given by Wróbel et al.[27] This leads to a Zeeman splitting energy $g^*\mu_BB$ of 0.34 meV in the channel. The Fermi level E_f and the exchange splitting energy Δ in the ferromagnetic contacts are set equal to 4.2 and 3.46 eV, respectively.[28]

The Rashba spin-orbit coupling strength α_R is typically derived from low-temperature magnetoresistance measurements (Shubnikov–de Haas oscillations) in two-dimensional electron gas (2DEG) created at the interface of semiconductor heterostructures.[29] To date, the largest reported experimental values of the Rashba spin-orbit coupling strength α_R have been found in InAs-based semiconductor heterojunctions. For a normal high electron mobility transistor (HEMT) In$_{0.75}$Al$_{0.25}$As/In$_{0.75}$Ga$_{0.25}$As heterojunction, Sato et al. have reported a variation of α_R from 30 to 15×10^{-12} eV m when the external gate voltage is swept from 0 to -6 V (the total electron concentration in the 2DEG is found to be reduced from 5 to 4.5×10^{11}/cm^2 over the same range of bias). For a channel length of 0.2 μm, this corresponds to a variation of the spin precession angle $\theta=2k_RL$ from about π to 0.5π over the same range of gate bias.

In the numerical results below, we calculated the conductance of a spin interferometer with a 0.2-μm-long channel as a function of the gate voltage at a temperature of 2 K.[30] Tuning the gate voltage varies both the potential energy barrier ΔE_c and the Rashba spin-orbit coupling strength α_R simultaneously.[31] Both of these variations lead to distinct types of conductance oscillations. The variation of ΔE_c causes the Fermi level in the channel to sweep through the resonant energies in the channel (resonant levels are caused by the potential steps at $x=0$ and $x=L$), causing the conductance to oscillate. These are known as Ramsauer oscillations (or Fabry-Perot-like resonances) and have been examined in the past by Matsuyama et al.[5] for two-dimensional structures and by us[32] for one-dimensional structures. The variation of α_R, on the other hand, causes spin precession in the channel, leading to the type of conductance oscillation which is the basis of the spin interferometer, as originally visualized by Datta and Das.[1] In Ref. 32 we found that the Ramsauer oscillations are much stronger and can mask the oscillations due to spin precession, unless the structure is designed with particular care to eliminate (or reduce) the Ramsauer oscillations. In the calculations reported here, we vary ΔE_c over a range of 10 meV which allows us to display several of the Ramsauer oscillations in the conductance. We are restricted to this range because we can increase ΔE_c at most by an amount equal to the Fermi energy in the channel. At the end of this range, the Fermi energy lines up with the conduction band edge in the channel which corresponds to onset of complete pinch-off; i.e., the channel carrier concentration falls to zero. Therefore, the maximum range of ΔE_c is the Fermi energy, as long as we are applying a negative gate voltage to deplete the channel as opposed to applying a positive gate voltage to accumulate the channel (we do not want to accumulate the channel since a large carrier concentration in the channel will lead to multiple subband occupation and will also ultimately shield the gate potential resulting in loss of gate control). In one-dimensional semiconductor channels, a realizable carrier concentration of $\sim6\times10^5$/cm, will correspond to a Fermi energy of 10 meV which also happens to
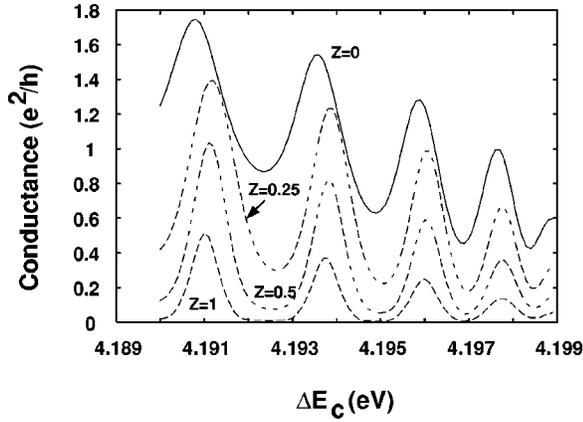
FIG. 3. Conductance modulation of a ballistic electron spin interferometer (for $T=2$ K) as the gate voltage (or the energy barrier ΔE_c) is varied. We assume that the Rashba coupling strength α_R varies from 30×10^{-12} eV m to 0 for the range of ΔE_c shown in the figure. This should correspond to one-half cycle of conductance oscillation due to spin precession. The separation between the two ferromagnetic contacts is 0.2 μm. The confinement energy $\hbar \omega$ along the z direction (direction transverse to both current flow and the gate electric field) is 10 meV. The conductance oscillations in this figure are caused by Fermi level sweeping through the resonant levels in the channel of the interferometer (the so-called Ramsauer effect) and are *not* due to the spin precession in the channel as shown in Ref. 32. The different curves correspond to different values of the parameter Z characterizing the strength of the interfacial barrier between the ferromagnetic contact and semiconducting channel. The semiconducting channel is assumed to be impurity free and, hence, ballistic.

be the subband separation energy $\hbar \omega$ in our case. Therefore, we restrict the Fermi energy to 10 meV in order to preserve single-subband occupancy, and this dictated our choice for the range of ΔE_c.

Over this range of ΔE_c, we assume that the Rashba spin-orbit coupling strength α_R varies from 30×10^{-12} eV m down to zero. This is consistent with experimentally observed dependence of α_R on gate voltage. This variation of α_R corresponds to a variation of the spin precession angle θ from about π to 0 (i.e., half a cycle of the oscillation expected from spin precession).

A. Influence of the interfacial barrier

The results of the conductance modulation are shown in Fig. 3 for different values of the parameter Z characterizing the strength of the δ barrier at the ferromagnet/semiconductor interface (assumed to be the same for both contacts). Instead of plotting the conductance as a function of gate voltage, we always plot it as a function of ΔE_c since ΔE_c directly enters the Hamiltonian in Eq. (4). The exact relationship between ΔE_c and the gate voltage is complicated by many factors (interface states, channel geometry, etc.), but for the sake of simplicity, we will assume that ΔE_c depends linearly on gate voltage. Therefore, the plots in Figs. 3–9 can be effectively viewed as plots of conductance versus gate voltage.
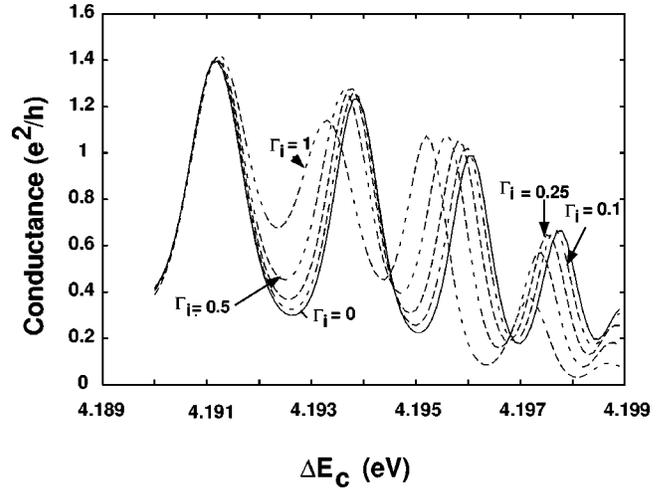

FIG. 4. Influence of a single impurity on the conductance modulation of an electron spin interferometer. All other parameters are the same as in Fig. 3. The interface potential at the ferromagnet/semiconductor interface is 2 eV Å corresponding to $Z=0.25$. The impurity is modeled as a repulsive δ scatterer with strength Γ_i indicated next to each curve in unit eV Å. The impurity is located 300 Å away from the left ferromagnetic contact/channel interface.

A value of $Z=1$ corresponds to a value of V_L and V_R in Eq. (2) equal to 8 eV Å. Figure 3 shows that the location of conductance minima and maxima are only slightly shifted along the ΔE_c axis with the variation of the parameter Z. The amplitudes of the oscillations increase with Z but then start to decrease as the maxima of the conductance is reduced for larger values of Z. This reduction in amplitude is expected since the conductance of the spin interferometer eventually reduces to zero as $Z \rightarrow \infty$ (no electron can enter or exit the channel if there are infinite barriers at the contact interface). The maximum in the conductance amplitude modulation occurs for $Z=0.25$ in our numerical examples. In the subse-
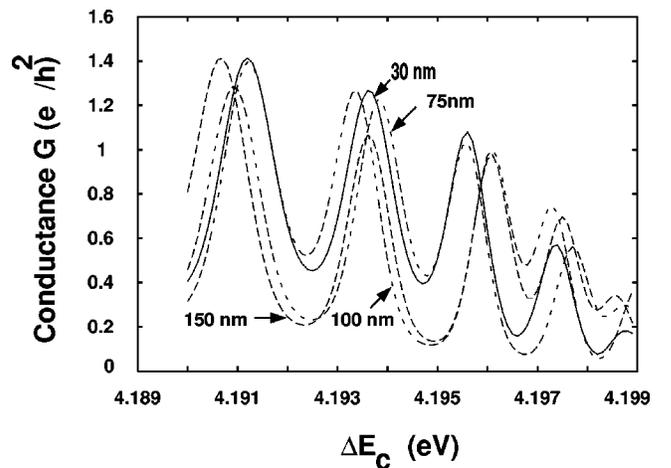

FIG. 5. Influence of a single impurity on the conductance modulation of an electron spin interferometer. Again, all other parameters are the same as in Fig. 3, and $Z=0.25$. The impurity is modeled as a repulsive δ scatterer with strength $\Gamma=0.5$ eV Å. Cases 1–4 correspond to an impurity located 300, 750, 1000, and 1500 Å away from the left ferromagnetic contact/channel interface.
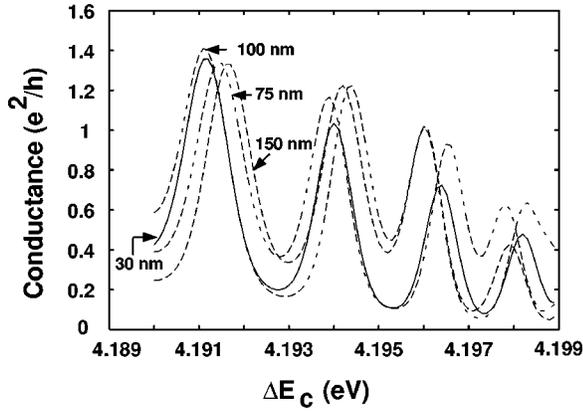
FIG. 6. Same as Fig. 5 for the case of an attractive impurity with strength $\Gamma = -0.5$ eV Å. Cases 1–4 correspond to an impurity located 300, 750, 1000, and 1500 Å away from the left ferromagnetic contact/channel interface.

FIG. 8. Same as Fig. 5 for the case of two attractive impurities with strength $\Gamma = -0.5$ eV Å. The curves labeled 1 and 2 correspond to the case of two impurities located at (300, 1000 Å) and (500, 1250 Å), from the left ferromagnet/channel interface, respectively.

quent numerical simulations which investigate the influence of impurity scattering on the conductance modulation, we therefore used $Z = 0.25$ throughout.

B. Impurity scattering

First, we consider the case of a single repulsive impurity at a fixed location within the channel (300 Å from the left ferromagnetic contact) but with varying strength Γ_i. Figure 4 shows that the size and location of the conductance peaks and minima are affected by the strength of the impurity scatterer and more strongly affected at larger values of ΔE_c. This is expected since the transmission probability through the impurity diminishes as the channel approaches pinch-off. Even though not shown here, the same trend was observed when the impurity was assumed to be an attractive scatterer (negative value for Γ_i). Figures 5 and 6 illustrate the dependence of the conductance of the interferometer on the exact location of an impurity with a scattering strength of $\Gamma_i = 0.5$ eV Å. Figures 5 and 6 correspond to the case of a repulsive and attractive impurities, respectively. These fig-
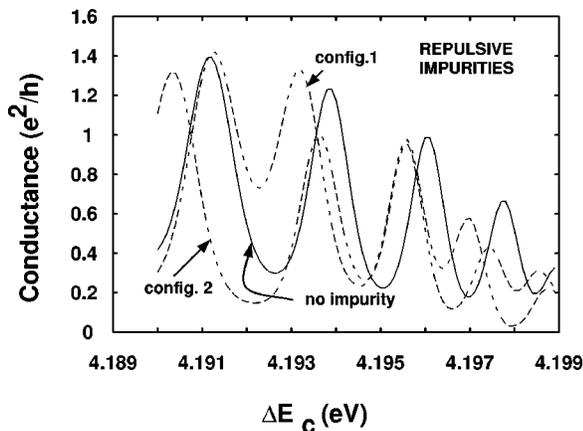
ures clearly show that the conductance modulation of the interferometer operating in a phase-coherent regime is affected by the exact location and strength of a single scatterer. In fact, Fig. 6 clearly shows that, if we change the location of the impurity, then the value of the conductance at a fixed value of ΔE_c changes by $\sim e^2/h$ which is reminiscent of the phenomenon of "universal conductance fluctuations."[33]

Next, we consider the case of two impurities in the channel at two different locations (300, 1000 Å) and (500, 1250 Å). The results for the cases of attractive and repulsive impurities (of equal strength) are shown in Figs. 7 and 8, respectively. These figures accentuate even more the features observed in Figs. 5 and 6—i.e., a strong dependence of the oscillation amplitude and phase (even far from pinch off) on

FIG. 9. Degree of spin-conductance polarization P vs ΔE_c. All other parameters are the same as listed in Fig. 3. The quantity P is plotted for the case of a ballistic channel with no impurity and also for the four two-impurity configurations (attractive and repulsive) considered in Figs. 7 and 8. The curves labeled 1 and 2 correspond to the case of two impurities located at (300, 1000 Å) and (500, 1250 Å), from the lef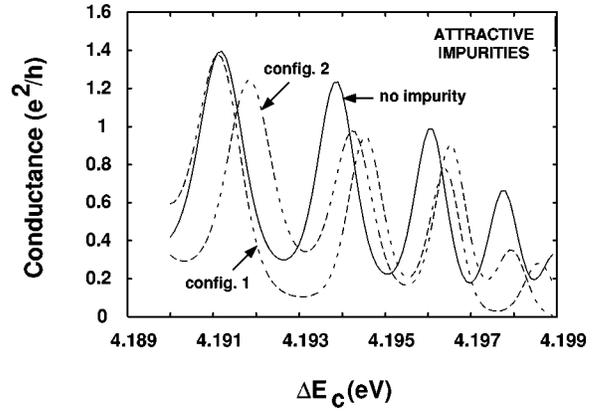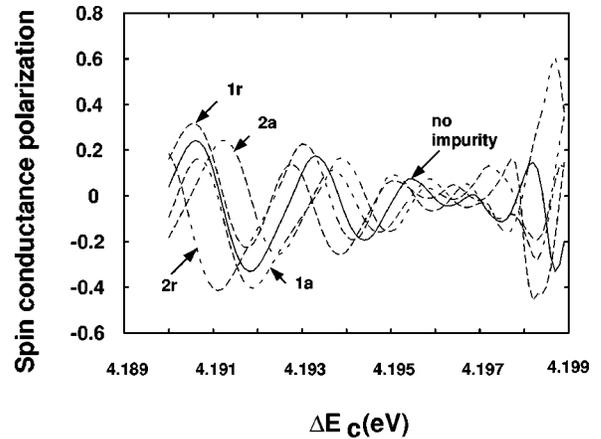t ferromagnet/channel interface, respectively. The extra labels r and a are to identify the case of repulsive and attractive scatterers, respectively.

FIG. 7. Same as Fig. 5 for the case of two repulsive impurities with strength $\Gamma = 0.5$ eV Å. The curves labeled 1 and 2 correspond to the case of two impurities located at (300, 1000 Å) and (500, 1250 Å), from the left ferromagnet/channel interface, respectively.

the impurity type and configurations. This sensitivity is due to the quantum interference between electron waves reflected multiple times between impurities and also between each impurity and the closest ferromagnetic contact. All these interferences affect the overall transmission probability of an electron through the interferometer and, hence, its conductance. These simulations show that, even if good ferromagnetic/semiconductor contacts with large degree of spin polarization can be realized through the use of an appropriate interfacial barrier, perfect control of the location of the conductance minima and maxima could still be elusive in the presence of just a few impurities in the channel. Obviously, this will have a deleterious effect on device reproducibility.

The strong sensitivity to the presence of impurities in the channel also has a profound influence on the spin-conductance polarization which is defined as[4]

$$P = \frac{G_{+x\text{-polarized}} - G_{-x\text{-polarized}}}{G_{+x\text{-polarized}} + G_{-x\text{-polarized}}}. \tag{23}$$

This quantity is plotted in Fig. 9 as a function of ΔE_c. The degree of spin polarization P is shown for the case of an impurity free channel and also for the four different two-impurity configurations (attractive and repulsive) considered in Figs. 7 and 8. This quantity takes both positive and negative values as the gate voltage is swept and reaches a maximum of 60% close to the threshold for channel pinch-off. However, near pinch-off, our model of impurity scattering should be modified to take into account the absence of screening at low carrier density. Even for a more refined model of impurity scattering, we believe that Fig. 9 is indicative of what is to be expected in realistic samples; i.e, the spin-conductance polarization is very sensitive to the nature and location of the impurities in the channel. The spin polarization therefore provides an actual fingerprint for each impurity configuration, a phenomenon similar to the universal conductance fluctuations linked to the displacement of a single impurity in mesoscopic samples.[33]

From an experimental point of view, the sensitivity of the spin-conductance polarization to the actual impurity configuration could be tested with experiments based on the Hanle effect, pioneered by Johnson and Silsbee[34] and later used by several groups.[35,36] For spin interferometers with very long channels and containing many impurities, the Hanle effect, which uses a small magnetic field perpendicular to the axis of magnetization of the ferromagnetic contacts, could be used to investigate the influence of the gate potential (via the Rashba effect) on the spin relaxation time T_2 of carriers in one-dimensional channels in the presence of an axial magnetic field.

IV. CONCLUSIONS

In this paper, we have developed a fully quantum mechanical approach to model-coherent electron spin transport in a disordered semiconductor channel using a particular model of impurity scattering. We have also shown how conductance modulation of the gate-controlled spin interferometers proposed in Ref. 1 is affected by the presence of interfacial barriers at the ferromagnetic contact/semiconductor interfaces and by a few impurities in the semiconducting channel. Quantum interference caused by multiple reflections of electron waves between impurities and between the impurities and the interfacial barriers can strongly affect the overall degree of spin polarization of the interferometer. The extreme sensitivity of the amplitude and phase of conductance oscillations to impurity location is reminiscent of the phenomenon of universal conductance fluctuations of mesoscopic samples. This will hinder practical applications of electron spin interferometers.

*Corresponding author. Electronic mail: marc.cahay@uc.edu

[1] S. Datta and B. Das, Appl. Phys. Lett. **56**, 665 (1990).

[2] E.I. Rashba, Sov. Phys. Semicond. **2**, 1109 (1960); Y.A. Bychkov and E.I. Rashba, J. Phys. C **17**, 6039 (1984).

[3] F. Mireles and G. Kirzcenow, Phys. Rev. B **64**, 024426 (2001).

[4] F. Mireles and G. Kirzcenow, Phys. Rev. B **66**, 214415 (2002).

[5] T. Matsuyama, C.-M. Hu, D. Grundler, G. Meier, and U. Merkt, Phys. Rev. B **65**, 155322 (2002).

[6] M.H. Larsen, A.M. Lunde, and K. Flensberg, Phys. Rev. B **66**, 033304 (2002).

[7] C.-T. Liang, M.Y. Simmons, C.G. Smith, D.A. Ritchie, and M. Pepper, Appl. Phys. Lett. **75**, 2975 (1999).

[8] R.J. Elliott, Phys. Rev. **96**, 266 (1954).

[9] V. Marigliano Ramaglia, V. Cataudella, G. De Filippis, C.A. Perroni, and F. Ventriglia, cond-mat/0203569 (unpublished).

[10] A.V. Moroz and C.H.W. Barnes, Phys. Rev. B **60**, 14 272 (1999); **61**, R2464 (2000).

[11] G. Lommer, F. Malcher, and U. Rössler, Phys. Rev. Lett. **60**, 728 (1988).

[12] B. Das, S. Datta, and R. Reifenberger, Phys. Rev. B **41**, 8278 (1990).

[13] Th. Schäpers, J. Nitta, H.B. Heersche, and H. Takayanagi, Phys. Rev. B **64**, 125314 (2001).

[14] E.I. Rashba, Phys. Rev. B **62**, 16 267 (2000).

[15] H. Sakaki, Jpn. J. Appl. Phys., Part 2 **19**, L735 (1980).

[16] G. Dresselhaus, Phys. Rev. **100**, 580 (1955).

[17] A. Bournel, V. Delmouly, P. Dollfus, G. Tremblay, and P. Hesto, Physica E (Amsterdam) **10**, 86 (2001); A. Bournel, P. Dollfus, P. Bruno, and P. Hesto, Eur. Phys. J.: Appl. Phys. **4**, 1 (1998).

[18] S. Saikin, M. Shen, M.-C. Cheng, and V. Privman, cond-mat/0212610 (unpublished).

[19] M. Shen, S. Saikin, M.-C. Cheng, and V. Privman, cond-mat/0302395 (unpublished).

[20] S. Pramanik, S. Bandyopadhyay, and M. Cahay, Phys. Rev. B **68**, 075313 (2003).

[21] M. Governale and U. Zülicke, Phys. Rev. B **66**, 073311 (2002).

[22] J. Carlos Egues, Phys. Rev. Lett. **80**, 4578 (1998).

[23] A.M. Kriman and P.P. Ruden, Phys. Rev. B **32**, 8013 (1985).

[24] R. Frohne and S. Datta, J. Appl. Phys. **64**, 4086 (1988).

[25] D. Grundler, Phys. Rev. B **63**, 161307(R) (2001).

[26] O.E. Raichev and P. Debray, Phys. Rev. B **65**, 085319 (2002).

[27] J. Wróbel, T. Dietl, K. Fronc, A. Lusakowski, M. Czeczott, G. Grabecki, R. Hey, and K.H. Ploog, Physica E (Amsterdam) **10**, 91 (2001).

[28] We use the same values as in F. Mireles and G. Kirczenow, Europhys. Lett. **59**, 107 (2002).

[29] J. Nitta, T. Akazaki, H. Takayanagi, and T. Enoki, Phys. Rev. Lett. **78**, 1335 (1997); G. Engels, J. Lange, Th. Schäpers, and H. Lüth, Phys. Rev. B **55**, 1958 (1997); Th. Schäpers, G. Engles, J. Lange, Th. Klocke, M. Hollfelder, and H. Lüth, J. Appl. Phys. **83**, 4324 (1998); C.-M. Hu, J. Nitta, T. Akazaki, H. Takayanagi, J. Osaka, P. Pfeffer, and W. Zawadzki, Phys. Rev. B **60**, 7736 (1999); J.P. Heida, B.J. van Wees, J.J. Kuipers, T.M. Kalpwijk, and G. Borghs, *ibid.* **57**, 11 911 (1998); S. Brosig, K. Ensslin, R.J. Warburton, C. Nguyen, B. Brar, M. Thomas, and H. Kroemer, *ibid.* **60**, 13 989 (1999); H.B. Heersche, Th. Schäpers, J. Nitta, and H. Takayanagi, *ibid.* **64**, 161307 (2001); Y. Sato, T. Kita, S. Gozu, and S. Yamada, J. Appl. Phys. **89**, 8017 (2001); Y. Sato, S. Gozu, T. Kita, and S. Yamada, Physica E (Amsterdam) **12**, 399 (2002).

[30] We compute the conductance using the Landauer formula by integrating over an energy range from $[E_f - 4k_BT, E_f + 4k_BT]$.

[31] It is possible, in principle, to arrange gates such that one can modulate the Rashba spin-orbit coupling without changing the net carrier concentration or ΔE_c. The Rashba effect responds to only the inversion asymmetric component of the gate electric field while the carrier concentration and ΔE_c respond to the total (symmetric plus asymmetric components) of the gate electric field. Therefore one could compensate for any change in the asymmetric component with an equivalent change in the symmetric component that will vary the Rashba effect without varying carrier concentration or ΔE_c.

[32] M. Cahay and S. Bandyopadhyay, Phys. Rev. B **68**, 115316 (2003).

[33] S.C. Feng, P.A. Lee, and A.D. Stone, Phys. Rev. Lett. **56**, 1960 (1986); P.A. Lee, A.D. Stone, and H. Fukuyama, Phys. Rev. B **35**, 1039 (1987); S. Datta, M. Cahay, and M. McLennan, *ibid.* **36**, 5655 (1987); M. Cahay, M. McLennan, and S. Datta, *ibid.* **37**, 10 125 (1988).

[34] M. Johnson and R.H. Silsbee, Phys. Rev. Lett. **55**, 1790 (1985).

[35] M. Johnson, Semicond. Sci. Technol. **17**, 298 (2002).

[36] F.J. Jedema, M.V. Costache, H.B. Heersche, J.J.A. Baselmans, and B.J. van Wees, Appl. Phys. Lett. **81**, 5162 (2002).

For each temperature, we limit the range of variation of ΔE_c so that both channels under the gate are conducting for the range of energy considered.